

# Covariant transport approach for strongly interacting partonic systems

W. Cassing<sup>1</sup> and E. L. Bratkovskaya<sup>2</sup>

<sup>1</sup>Institut für Theoretische Physik, Universität Giessen, Germany

<sup>2</sup>Institut für Theoretische Physik, Universität Frankfurt am Main, Germany

E-mail: Wolfgang.Cassing@theo.physik.uni-giessen.de

**Abstract.** The dynamics of partons, hadrons and strings in relativistic nucleus-nucleus collisions is analyzed within the novel Parton-Hadron-String Dynamics (PHSD) transport approach, which is based on a dynamical quasiparticle model for partons (DQPM) matched to reproduce recent lattice-QCD results - including the partonic equation of state - in thermodynamic equilibrium. Scalar- and vector-interaction densities are extracted from the DQPM as well as effective scalar- and vector-mean fields for the partons. The transition from partonic to hadronic degrees of freedom is described by covariant transition rates for the fusion of quark-antiquark pairs or three quarks (antiquarks), respectively, obeying flavor current-conservation, color neutrality as well as energy-momentum conservation. Since the dynamical quarks and antiquarks become very massive close to the phase transition, the formed resonant 'pre-hadronic' color-dipole states ( $q\bar{q}$  or  $qqq$ ) are of high invariant mass, too, and sequentially decay to the groundstate meson and baryon octets increasing the total entropy. When applying the PHSD approach to Pb+Pb collisions at 158 A·GeV we find a significant effect of the partonic phase on the production of multi-strange antibaryons due to a slightly enhanced  $s\bar{s}$  pair production from massive time-like gluon decay and a larger formation of antibaryons in the hadronization process.

## 1. Introduction

The 'Big Bang' scenario implies that in the first micro-seconds of the universe the entire state has emerged from a partonic system of quarks, antiquarks and gluons – a quark-gluon plasma (QGP) – to color neutral hadronic matter consisting of interacting hadronic states (and resonances) in which the partonic degrees of freedom are confined. The nature of confinement and the dynamics of this phase transition has motivated a large community for several decades and is still an outstanding question of today's physics. Early concepts of the QGP were guided by the idea of a weakly interacting system of partons which might be described by perturbative QCD (pQCD). However, experimental observations at the Relativistic Heavy Ion Collider (RHIC) indicated that the new medium created in ultrarelativistic Au+Au collisions is interacting more strongly than hadronic matter and consequently this concept had to be severely questioned. Moreover, in line with theoretical studies in Refs. [1, 2, 3] the medium showed phenomena of an almost perfect liquid of partons [4, 5] as extracted from the strong radial expansion and the scaling of elliptic flow  $v_2(p_T)$  of mesons and baryons with the number of constituent quarks and antiquarks [4].

The question about the properties of this (nonperturbative) QGP liquid is discussed controversially in the literature and dynamical concepts describing the formation of color neutral

hadrons from colored partons are scarce. A fundamental issue for hadronization models is the conservation of 4-momentum as well as the entropy problem because by fusion/coalescence of massless (or low constituent mass) partons to color neutral bound states of low invariant mass (e.g. pions) the number of degrees of freedom and thus the total entropy is reduced in the hadronization process [6, 7, 8]. This problem - a violation of the second law of thermodynamics as well as the conservation of four-momentum and flavor currents - has been addressed in Ref. [9] on the basis of the DQPM employing covariant transition rates for the fusion of 'massive' quarks and antiquarks to color neutral hadronic resonances or strings. In fact, the dynamical studies for an expanding partonic fireball in Ref. [9] suggest that the latter problems have come to a practical solution.

A consistent dynamical approach - valid also for strongly interacting systems - can be formulated on the basis of Kadanoff-Baym (KB) equations [10] or off-shell transport equations in phase-space representation, respectively [10, 11, 12]. In the KB theory the field quanta are described in terms of dressed propagators with complex selfenergies. Whereas the real part of the selfenergies can be related to mean-field potentials (of Lorentz scalar, vector or tensor type), the imaginary parts provide information about the lifetime and/or reaction rates of time-like 'particles' [13]. Once the proper (complex) selfenergies of the degrees of freedom are known the time evolution of the system is fully governed by off-shell transport equations (as described in Refs. [10, 13]). The determination/extraction of complex selfenergies for the partonic degrees of freedom has been performed before in Refs. [14, 15] by fitting lattice QCD (lQCD) 'data' within the Dynamical QuasiParticle Model (DQPM). In fact, the DQPM allows for a simple and transparent interpretation of lattice QCD results for thermodynamic quantities as well as correlators and leads to effective strongly interacting partonic quasiparticles with broad spectral functions. For a review on off-shell transport theory and results from the DQPM in comparison to lQCD we refer the reader to Ref. [13].

In the present contribution we will report on an update of the DQPM parameters [16] since more precise lQCD calculations for 2+1 flavors with almost physical quark masses have become available in 2008 [17]. Furthermore, we extend the study in Refs. [14, 15] by fixing independently scalar- and vector-interaction densities for the fermion degrees of freedom. First applications of the PHSD approach to Pb +Pb collisions at SPS energies - in comparison to experimental data from the NA49 Collaboration - are presented, too.

## 2. The PHSD approach

The Parton-Hadron-String-Dynamics (PHSD) approach is a microscopic covariant transport model that incorporates effective partonic as well as hadronic degrees of freedom and involves a dynamical description of the hadronization process from partonic to hadronic matter. Whereas the hadronic part is essentially equivalent to the conventional Hadron-Strings-Dynamics (HSD) approach [18] the partonic dynamics is based on the Dynamical QuasiParticle Model (DQPM) [14, 15] which describes QCD properties in terms of single-particle Green's functions (in the sense of a two-particle irreducible (2PI) approach).

### 2.1. Reminder of the DQPM

We briefly recall the basic assumptions of the DQPM: Following Ref. [19] the dynamical quasiparticle mass (for gluons and quarks) is assumed to be given by the thermal mass in the asymptotic high-momentum regime, which is proportional to the coupling  $g(T/T_c)$  and the temperature  $T$ , i.e. for gluons

$$M_g^2(T) = \frac{g^2(T/T_c)}{6} \left( (N_c + \frac{1}{2}N_f) T^2 + \frac{N_c}{2} \sum_q \frac{\mu_q^2}{\pi^2} \right), \quad (1)$$

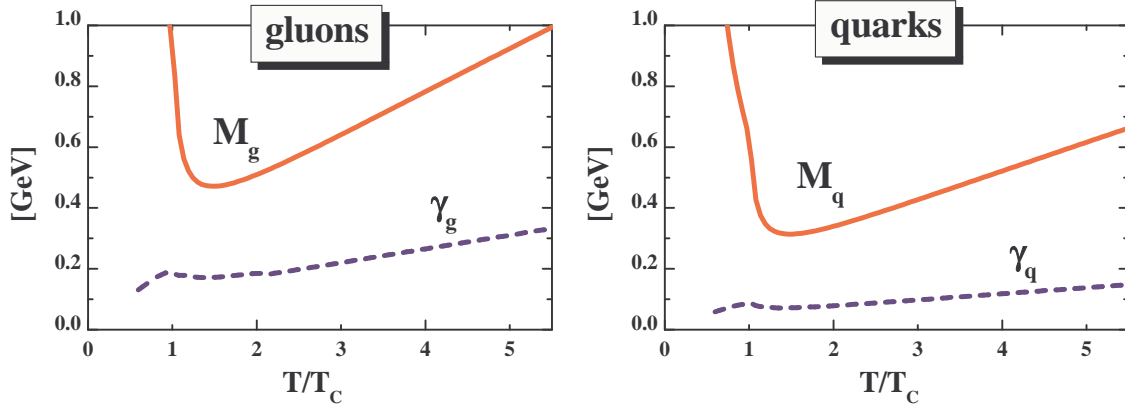


**Figure 1.** The effective gluon mass  $M_g$  and width  $\gamma_g$  as function of temperature  $T/T_c$  (l.h.s.). The r.h.s. shows the corresponding quantities for quarks.

and for quarks (assuming vanishing constituent masses here) as,

$$M_q^2(T) = \frac{N_c^2 - 1}{8N_c} g^2(T/T_c) \left( T^2 + \frac{\mu_q^2}{\pi^2} \right), \quad (2)$$

with a running coupling (squared) (for  $T > T_s$ ),

$$g^2(T/T_c) = \frac{48\pi^2}{(11N_c - 2N_f) \ln(\lambda^2(T/T_c - T_s/T_c)^2)}, \quad (3)$$

which permits for an enhancement near the critical temperature  $T_c$ . Here  $N_c = 3$  stands for the number of colors while  $N_f$  denotes the number of flavors. The parameters controlling the infrared enhancement of the coupling  $\lambda$  and  $T_s$  have been refitted compared to Ref. [19] to the recent lQCD results from Ref. [17] (see below).

The width for gluons and quarks (for  $\mu_q = 0$ ) is adopted in the form [20]

$$\gamma_g(T) = N_c \frac{g^2 T}{8\pi} \ln \frac{2c}{g^2}, \quad \gamma_q(T) = \frac{N_c^2 - 1}{2N_c} \frac{g^2 T}{8\pi} \ln \frac{2c}{g^2}. \quad (4)$$

where the parameter  $c$  is related to a magnetic cut-off. We stress that a non-vanishing width  $\gamma$  is the central difference of the DQPM to conventional quasiparticle models [21, 22]. Its influence is essentially seen in correlation functions as e.g. in the stationary limit of the correlation function in the off-diagonal elements of the energy-momentum tensor  $T^{kl}$  which defines the shear viscosity  $\eta$  of the medium [3, 23]. Here a sizable width is mandatory to obtain a small ratio in the shear viscosity to entropy density  $\eta/s$  [3].

The actual gluon mass  $M_g$  and width  $\gamma_g$  – employed in the further calculations – as well as the quark mass  $M_q$  and width  $\gamma_q$  are depicted in Fig. 1 on the lhs and rhs, respectively, as a function of  $T/T_c$ . These values for the masses and widths are smaller than those presented in Ref. [19] since the recent lQCD calculations [17] have been performed with much smaller bare fermion masses. This, in fact, leads to an increase in the entropy density  $s(T/T_c)$  relative to earlier lQCD calculations, which implies that the quasiparticle mass and width - fitting the lQCD results - become smaller relative to Refs. [14, 15, 19].

In line with Ref. [19] the parton spectral functions are no longer  $\delta$ - functions in the invariant mass squared but taken as

$$\rho_j(\omega) = \frac{\gamma_j}{E_j} \left( \frac{1}{(\omega - E_j)^2 + \gamma_j^2} - \frac{1}{(\omega + E_j)^2 + \gamma_j^2} \right) \quad (5)$$

separately for quarks and gluons ( $j = q, \bar{q}, g$ ). With the convention  $E^2(\mathbf{p}) = \mathbf{p}^2 + M_j^2 - \gamma_j^2$ , the parameters  $M_j^2$  and  $\gamma_j$  are directly related to the real and imaginary parts of the retarded self-energy, e.g.  $\Pi_j = M_j^2 - 2i\gamma_j\omega$ . The spectral function (5) is antisymmetric in  $\omega$  and normalized as

$$\int_{-\infty}^{\infty} \frac{d\omega}{2\pi} \omega \rho_j(\omega, \mathbf{p}) = \int_0^{\infty} \frac{d\omega}{2\pi} 2\omega \rho_j(\omega, \mathbf{p}) = 1. \quad (6)$$

With the spectral functions fixed by Eqs. (1)-(5) the total energy density in the DQPM  $T_+^{00} + T_-^{00}$  can be evaluated as [15]

$$\begin{aligned} T_{\pm}^{00} &= d_g \int_0^{\infty} \frac{d\omega}{2\pi} \int \frac{d^3p}{(2\pi)^3} 2\omega^2 \rho_g(\omega, \mathbf{p}) n_B(\omega/T) \Theta(\pm p^2) \\ &+ d_q \int_0^{\infty} \frac{d\omega}{2\pi} \int \frac{d^3p}{(2\pi)^3} 2\omega^2 \rho_q(\omega, \mathbf{p}) n_F((\omega - \mu_q)/T) \Theta(\pm p^2) \\ &+ d_{\bar{q}} \int_0^{\infty} \frac{d\omega}{2\pi} \int \frac{d^3p}{(2\pi)^3} 2\omega^2 \rho_{\bar{q}}(\omega, \mathbf{p}) n_F((\omega + \mu_q)/T) \Theta(\pm p^2), \end{aligned} \quad (7)$$

where  $n_B$  and  $n_F$  denote the Bose and Fermi functions, respectively, while  $\mu_q$  stands for the quark chemical potential. The number of transverse gluonic degrees of freedom is  $d_g = 16$  while the fermion degrees of freedom amount to  $d_q = d_{\bar{q}} = 2N_c N_f = 18$  in case of three flavors ( $N_f=3$ ). The indices  $\pm$  stand for the time-like (+) and space-like part (-) of the energy density (7) as defined via  $\Theta(\pm p^2)$  with  $p^2 = \omega^2 - \mathbf{p}^2$ .

The pressure  $P(T)$  then can be obtained by integrating the differential thermodynamic relation (for  $\mu_q = 0$ )

$$P - T \frac{\partial P}{\partial T} = -T^{00} = P - T s \quad (8)$$

with the entropy density  $s(T)$  given by

$$s = \frac{\partial P}{\partial T} = \frac{T^{00} + P}{T}. \quad (9)$$

This approach is thermodynamically consistent and represents a two-particle irreducible (2PI) approximation to hot QCD.

For the further presentation of the DQPM it is useful to introduce the shorthand notations (following Ref. [15])

$$\begin{aligned} \tilde{\text{Tr}}_g^{\pm} \dots &= d_g \int \frac{d\omega}{2\pi} \frac{d^3p}{(2\pi)^3} 2\omega \rho_g(\omega) \Theta(\omega) n_B(\omega/T) \Theta(\pm p^2) \dots \\ \tilde{\text{Tr}}_q^{\pm} \dots &= d_q \int \frac{d\omega}{2\pi} \frac{d^3p}{(2\pi)^3} 2\omega \rho_q(\omega) \Theta(\omega) n_F((\omega - \mu_q)/T) \Theta(\pm p^2) \dots \\ \tilde{\text{Tr}}_{\bar{q}}^{\pm} \dots &= d_{\bar{q}} \int \frac{d\omega}{2\pi} \frac{d^3p}{(2\pi)^3} 2\omega \rho_{\bar{q}}(\omega) \Theta(\omega) n_F((\omega + \mu_q)/T) \Theta(\pm p^2) \dots \end{aligned} \quad (10)$$

with  $p^2 = \omega^2 - \mathbf{p}^2$  denoting the invariant mass squared. Here the  $\Theta(\pm p^2)$ -functions project on 'time-like' (+) and 'space-like' (-) sectors of the four-momentum. The traces in (10) then give directly time-like and space-like 'densities' for gluons  $N_g^{\pm}$  as well as for quarks  $N_q^{\pm}$  (and antiquarks). Note, that only the time-like parts have the physical interpretation of particles per volume. We mention that scalar gluon and quark (+antiquark) densities are evaluated as

$$\rho_g^s\left(\frac{T}{T_c}\right) = \text{Tr}_g^+ \left( \frac{\sqrt{p^2}}{\omega} \right), \quad \rho_q^s\left(\frac{T}{T_c}\right) = \text{Tr}_q^+ \left( \frac{\sqrt{p^2}}{\omega} \right) + \text{Tr}_{\bar{q}}^+ \left( \frac{\sqrt{p^2}}{\omega} \right). \quad (11)$$

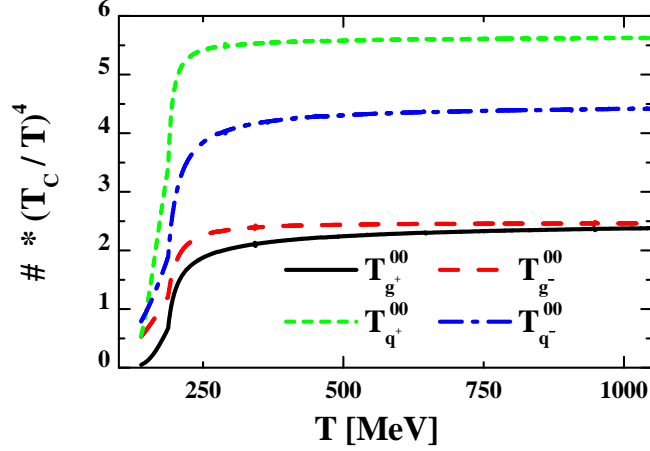


**Figure 2.** The different time- and space-like contributions to the total energy density as a function of  $T/T_c$  in units of  $\text{GeV}/\text{fm}^3$ . All quantities here have been multiplied by  $(T_c/T)^4$  to map out the scaling properties with temperature  $T$ .

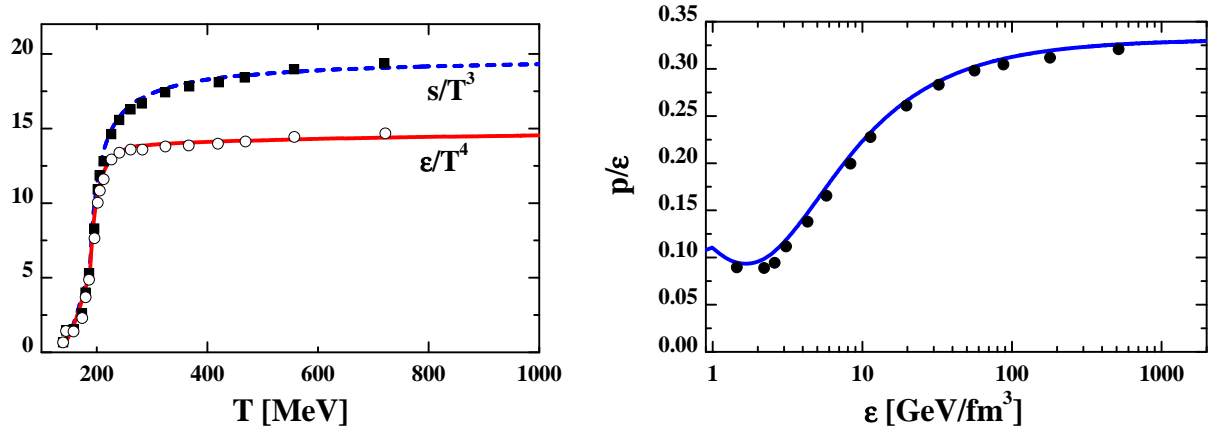


**Figure 3.** Lhs: The entropy density  $s(T)$  (dashed line) and energy density  $\epsilon(T)$  (solid line) from the DQPM in comparison to the IQCD results from Ref. [17] (full squares and open dots). Rhs: The equation-of-state (solid line) from the DQPM in comparison to the IQCD results from Ref. [17] (full dots).

As seen from Fig. 2 in Ref. [16] the 'densities' roughly scale with  $(T/T_c)^3$  except for the region close to  $T_c$ .

The time- and space-like energy densities  $T_{\pm}^{00}$  for gluons and quarks (+ antiquarks) are displayed in Fig. 2 as a function of  $T/T_c$  for the present parameter set in units of  $\text{GeV}/\text{fm}^3$ . The space-like energy density for gluons is slightly larger than the time-like part whereas the fermion contribution (quarks + antiquarks) is clearly dominated by the time-like sector. All quantities roughly scale as  $(T/T_c)^4$  except for the region close to  $T_c$ .

A direct comparison of the entropy density  $s(T)$  and energy density  $\epsilon(T)$  from the DQPM with results from IQCD from Ref. [17] is presented in Fig. 3 (lhs). Both results have been divided by  $T^3$  and  $T^4$ , respectively, to demonstrate the scaling with temperature. We briefly note that the agreement is sufficiently good. This also holds for the 'equation of state', i.e.  $P/\epsilon$  versus  $\epsilon$  as demonstrated in Fig. 3 (rhs).

As discussed in detail in Refs. [14, 15] and explicitly addressed in Eq. (7), the energy-density functional can be separated in space-like and time-like sectors when the spectral functions acquire a finite width. The space-like (-) part of (7)

$$V_p(T, \mu_q) = T_{g^-}^{00} + T_{q^-}^{00} + T_{\bar{q}^-}^{00} \quad (12)$$

may be interpreted as a potential-energy density  $V_p$  since the field quanta involved are virtual and correspond to partons exchanged in interaction diagrams. The time-like part (+) of (7) corresponds to effective field quanta which can be propagated within the light-cone. Without repeating the details we mention that mean-field potentials for partons can be defined by the derivative of the potential-energy density  $V_p$  with respect to the time-like parton densities and effective interactions by second derivatives of  $V_p$  (cf. Section 3 in Ref. [15]).

In analogy to relativistic effective approaches for nucleonic degrees of freedom [24, 25] we assume the potential energy density (12) to be a sum of scalar and vector parts, i.e.

$$V_p(T, \mu_q) = V_s(T, \mu_q) + V_v(T, \mu_q) . \quad (13)$$

In the dynamical quasiparticle picture the pressure  $P$  then is a sum of kinetic as well as interaction parts, i.e.

$$P(T, \mu_q) = \langle P_{xx} \rangle_{T, \mu_q} - V_s(T, \mu_q) + V_v(T, \mu_q) \quad (14)$$

with

$$\langle P_{xx} \rangle_{T, \mu_q} = \frac{1}{3} \left( Tr_g^+ \left( \frac{\mathbf{p}^2}{\omega} \right) + Tr_q^+ \left( \frac{\mathbf{p}^2}{\omega} \right) + Tr_{\bar{q}}^+ \left( \frac{\mathbf{p}^2}{\omega} \right) \right) . \quad (15)$$

In a similar way the total energy density  $\epsilon$  can be expressed as

$$\epsilon(T, \mu_q) = \langle \omega \rangle_{T, \mu_q} + V_s(T, \mu_q) + V_v(T, \mu_q) \quad (16)$$

with the time-like quasiparticle energy density given by

$$\langle \omega \rangle_{T, \mu_q} = Tr_g^+ (\omega) + Tr_q^+ (\omega) + Tr_{\bar{q}}^+ (\omega) . \quad (17)$$

Note the different signs for the scalar interaction part in (14) and (16) which stem from the metric tensor in the energy-momentum tensor  $T^{\mu\nu}$ . Since the total energy density as well as pressure are known in the DQPM and the kinetic parts (15) and (16) can be evaluated as well, the vector and scalar interaction densities can be uniquely extracted from the equations above. The corresponding results are displayed in Fig. 4 (lhs) for the total interaction per scalar particle  $V_p/\rho_s$  (upper dot-dashed line) and its decomposition in scalar (solid line) and vector (dashed line) parts as a function of the scalar parton density  $\rho_s$ ,

$$\rho_s = \rho_g^s + \rho_q^s + \rho_{\bar{q}}^s, \quad (18)$$

which is a convenient (Lorentz invariant) quantity to characterize the system instead of the Lagrange parameters  $T^{-1}$  and  $\mu_q$ . In fact, as found in Ref. [13] the thermodynamic quantities for different  $T$  and  $\mu_q$  are very close when representing them as a function of  $\rho_s$  or the parton density  $\rho_p$ , respectively.

Scalar and vector mean-field potentials are defined by derivatives of  $V_s$  and  $V_v$  with respect to the densities  $\rho_s$  and  $\rho_v$ , respectively,

$$U_s(\rho_s) = \frac{\partial V_s}{\partial \rho_s}; \quad U_v^0 = \frac{\partial V_v}{\partial \rho_p} . \quad (19)$$

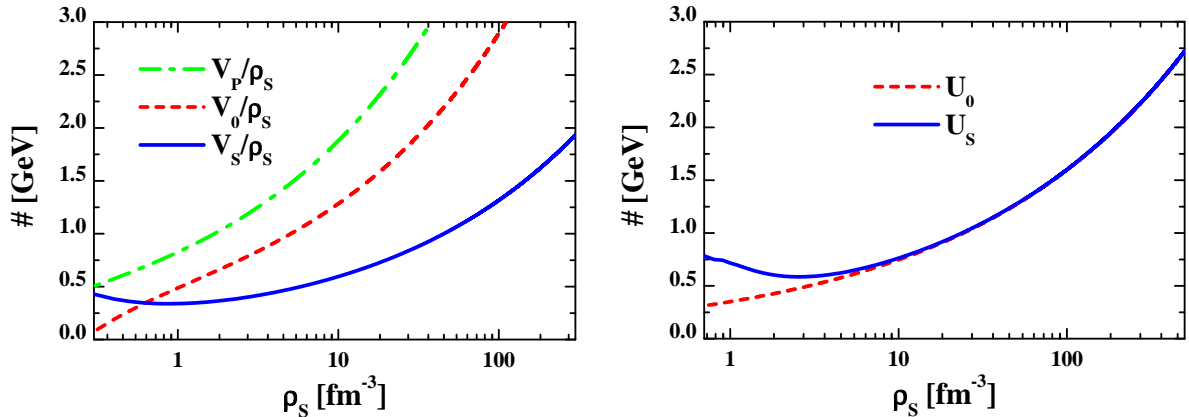


**Figure 4.** Lhs: The total potential energy per scalar parton (green dashed-dotted line) separated into scalar (solid blue line) and vector (red dashed line) parts (see text) as a function of the scalar parton density  $\rho_s$ . Rhs: The scalar (blue solid line) and vector (red dashed line) mean-fields for quarks (19) as a function of the scalar parton density  $\rho_s$ .

Both quantities (after differentiation) may be considered as a function of the parton-scalar density  $\rho_s$ . The resulting functions are displayed in Fig. 4 (rhs) as a function of  $\rho_s$  and show approximately equal results at high scalar density (or energy density, respectively). The low-density properties, however, are very different. Whereas the vector-mean field drops to zero with decreasing  $\rho_s$  the scalar-mean field increases substantially below  $\rho_s \approx 1 \text{ fm}^{-3}$ ; it very smoothly increases with density for  $\rho_s > 2 \text{ fm}^{-3}$ <sup>1</sup>. Accordingly scalar forces on the partons  $\sim -\partial U_s/\partial \rho_s \nabla \rho_s$  are rather small in the high-density partonic phase and only become stronger in the low-density phase close to hadronization. The DQPM as well as lQCD do not allow to extrapolate  $U_s$  down to  $\rho_s = 0$  reliably but one might imagine that  $U_s(\rho_s \rightarrow 0) \rightarrow \infty$  thus encoding scalar confinement on the mean-field level. We note that in actual PHSD calculations such low partonic densities are not probed dynamically because the partons hadronize in the region  $\rho_s \approx 1$  to  $2 \text{ fm}^{-3}$  (see below).

With the scalar- and vector-mean fields fixed for the partons (assuming the gluon mean fields to be twice the quark mean fields according to the analysis within the DQPM (cf. Ref. [15]) and with the effective masses and dynamical widths fixed by the DQPM (as a function of  $\rho_s$  instead of  $(T/T_c)$ ) the mean-field propagation of partons in PHSD is fully determined by the off-shell transport equations (cf. the review [13]). Note that these mean-fields are presently momentum independent whereas nuclear physics studies suggest a moderate dependence on the particle momentum [26, 27].

The transport equations still require to specify the elastic and inelastic cross sections of quarks and gluons, which enter the collision terms. For the latter quantities we refer the reader to Ref. [16].

## 2.2. Hadronization in PHSD

The hadronisation, i.e. the transition from partonic to hadronic degrees of freedom, is described in PHSD by local covariant transition rates as introduced in Ref. [9] e.g. for  $q + \bar{q}$  fusion to a meson  $m$  of four-momentum  $p = (\omega, \mathbf{p})$  at space-time point  $x = (t, \mathbf{x})$ :

$$\frac{dN_m(x, p)}{d^4x d^4p} = Tr_q Tr_{\bar{q}} \delta^4(p - p_q - p_{\bar{q}}) \delta^4\left(\frac{x_q + x_{\bar{q}}}{2} - x\right)$$

<sup>1</sup> Note the logarithmic scale in  $\rho_s$ .

$$\begin{aligned} & \times \omega_q \rho_q(p_q) \omega_{\bar{q}} \rho_{\bar{q}}(p_{\bar{q}}) |v_{q\bar{q}}|^2 W_m(x_q - x_{\bar{q}}, (p_q - p_{\bar{q}})/2) \\ & \times N_q(x_q, p_q) N_{\bar{q}}(x_{\bar{q}}, p_{\bar{q}}) \delta(\text{flavor, color}). \end{aligned} \quad (20)$$

In Eq. (20) we have introduced the shorthand notation,

$$Tr_j = \sum_j \int d^4x_j \int \frac{d^4p_j}{(2\pi)^4}, \quad (21)$$

where  $\sum_j$  denotes a summation over discrete quantum numbers (spin, flavor, color);  $N_j(x, p)$  is the phase-space density of parton  $j$  at space-time position  $x$  and four-momentum  $p$ . In Eq. (20)  $\delta(\text{flavor, color})$  stands symbolically for the conservation of flavor quantum numbers as well as color neutrality of the formed hadron  $m$  which can be viewed as a color-dipole or 'pre-hadron'. Furthermore,  $v_{q\bar{q}}(\rho_p)$  is the effective quark-antiquark interaction from the DQPM (displayed in Fig. 10 of Ref. [15]) as a function of the local parton ( $q + \bar{q} + g$ ) density  $\rho_p$  (or energy density). Furthermore,  $W_m(x, p)$  is the dimensionless phase-space distribution of the formed 'pre-hadron', i.e.

$$W_m(\xi, p_\xi) = \exp\left(\frac{\xi^2}{2b^2}\right) \exp\left(2b^2(p_\xi^2 - (M_q - M_{\bar{q}})^2/4)\right) \quad (22)$$

with  $\xi = x_1 - x_2 = x_q - x_{\bar{q}}$  and  $p_\xi = (p_1 - p_2)/2 = (p_q - p_{\bar{q}})/2$  (which has been previously introduced in Eq. (2.14) of Ref. [28]). The width parameter  $b$  is fixed by  $\sqrt{\langle r^2 \rangle} = b = 0.66$  fm (in the rest frame) which corresponds to an average rms radius of mesons. We note that the expression (22) corresponds to the limit of independent harmonic oscillator states and that the final hadron-formation rates are approximately independent of the parameter  $b$  within reasonable variations. By construction the quantity (22) is Lorentz invariant; in the limit of instantaneous 'hadron formation', i.e.  $\xi^0 = 0$ , it provides a Gaussian dropping in the relative distance squared  $(\mathbf{r}_1 - \mathbf{r}_2)^2$ . The four-momentum dependence reads explicitly (except for a factor 1/2)

$$(E_1 - E_2)^2 - (\mathbf{p}_1 - \mathbf{p}_2)^2 - (M_1 - M_2)^2 \leq 0 \quad (23)$$

and leads to a negative argument of the second exponential in (22) favoring the fusion of partons with low relative momenta  $p_q - p_{\bar{q}} = p_1 - p_2$ .

Related transition rates (to Eq. (20)) are defined for the fusion of three off-shell quarks ( $q_1 + q_2 + q_3 \leftrightarrow B$ ) to color neutral baryonic ( $B$  or  $\bar{B}$ ) resonances of finite width (or strings) fulfilling energy and momentum conservation as well as flavor current conservation using Jacobi coordinates (cf. Ref. [16]).

On the hadronic side the PHSD transport approach includes explicitly the baryon octet and decouplet, the  $0^-$ - and  $1^-$ -meson nonets as well as selected higher resonances as in HSD [18]. Hadrons of higher masses ( $> 1.5$  GeV in case of baryons and  $> 1.3$  GeV in case of mesons) are treated as 'strings' (color-dipoles) that decay to the known (low-mass) hadrons according to the JETSET algorithm [29]. We discard an explicit recapitulation of the string decay and refer the reader to the original work [29] or Ref. [30].

### 3. Application to nucleus-nucleus collisions

In this Section we employ the PHSD approach - described in Section 2 - to nucleus-nucleus collisions at moderate relativistic energies, i.e. at SPS energies where our approximations are expected to work. Note that at RHIC or LHC energies other initial conditions (e.g. a color-glass condensate [31]) might be necessary. Since this is a slightly different subject we here restrict to bombarding energies below 160 A·GeV where such problems/questions are expected to be not relevant.

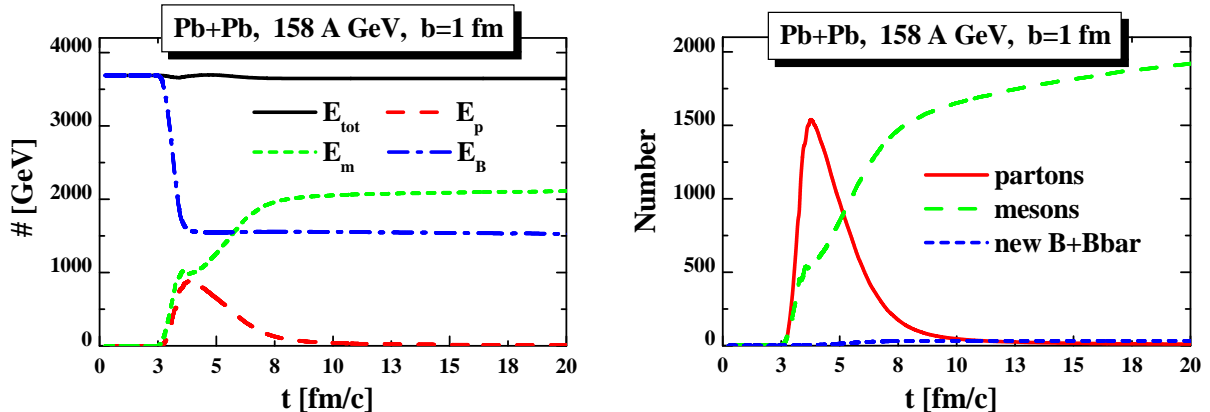


**Figure 5.** Lhs: The total energy  $E_{tot}$  (upper solid line) for central ( $b=1$  fm) collisions of Pb+Pb at 158 A·GeV. The long-dashed (red) line shows the energy contributions  $E_p$  from partons while the short-dashed (green) line displays the energy contribution from mesons  $E_m$  (including 'unformed mesons' in strings). The dot-dashed (blue) line is the contribution of baryons (and antibaryons)  $E_B$ ; the difference between the initial baryonic energy  $E_B(t=0)$  and final baryonic energy  $E_B(t \rightarrow \infty)$  gives the energy that is converted during the heavy-ion collision to final mesonic states. Rhs: The number of produced partons (solid red line), mesons (long dashed green line) and newly produced baryon + antibaryons (blue dashed line) as a function of time for Pb+Pb at 158 A·GeV (for  $b=1$  fm). Note that the number of mesons still increases for  $t > 20$  fm/c due to the decay of vector mesons.

### 3.1. Partonic energy fractions

We start with a consideration of energy partitions in order to map out the fraction of partonic energy in time for relativistic nucleus-nucleus collisions. In Fig. 5 (lhs) we show the energy balance for a central (impact parameter  $b=1$  fm) reaction of Pb+Pb at 158 A · GeV, i.e. at the top SPS energy. The total energy  $E_{tot}$  (upper line) - which at  $t=0$  is given by the energy of the colliding nuclei in the cms - is conserved throughout the reaction, i.e. in the partonic and hadronization phase as well as in the hadronic phase. Whereas in the first  $\sim 3$  fm/c the total energy is entirely contained in the impinging nucleons (including about 6 MeV per nucleon of binding energy) a rapid transition to partonic degrees of freedom is seen at  $t \approx 3$  fm/c, i.e. when the nuclei have started to overlap and react. We recall that the transition time of the two Pb-nuclei is about  $2R_{Pb}/\gamma_{cm} \approx 1.5$  fm/c at the top SPS energy. During this time period about 60% of initial kinetic energy of nucleons is converted to partons (red dashed line) and to mesons (short dashed green line) in the surface region ('corona') of the colliding system. Note that in the 'mesonic' energy  $E_m$  also 'unformed mesons' - as fragments of the strings - are accounted for. The energy of residual baryons (including antibaryons) is shown in terms of the dot-dashed (blue) line and is almost constant for  $t > 5$  fm/c implying that the various final-state interactions do not show up significantly in the energy fractions. The partonic phase - in a limited space-time region - approximately ends for  $t > 9$  fm/c which means that the further time evolution of the system is essentially described by hadronic interactions (HSD). Note that a sizeable fraction of energy is asymptotically still contained in the baryons. Since the baryon-rest masses amount to an energy of about 449 GeV (including newly produced  $B\bar{B}$  pairs) this implies that full stopping is not achieved in central Pb+Pb collisions at 158 A · GeV.

Let's have a closer look at the 'particle' composition in time for this reaction. We concentrate on those species that carry the energy transferred during the collision to new degrees of freedom. In this respect we display in Fig. 5 (rhs) the number of produced partons (solid red line), mesons

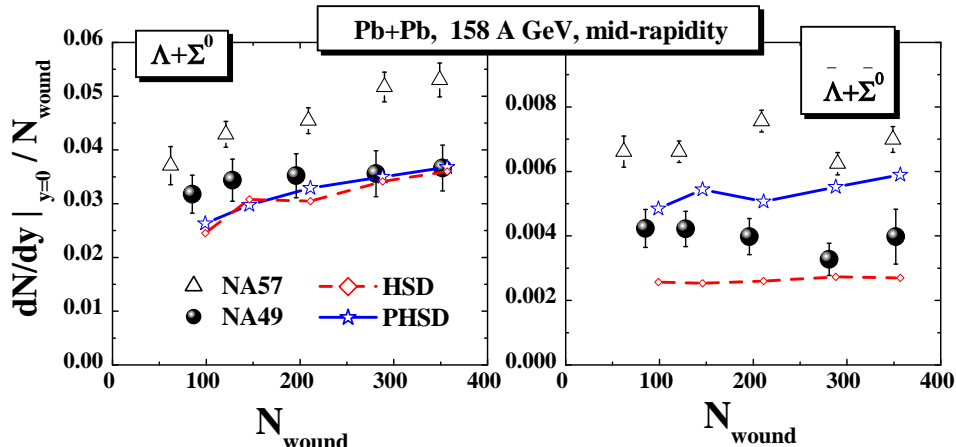


**Figure 6.** The multiplicities of  $(\Lambda + \Sigma^0)/N_{wound}$  (l.h.s.) and  $(\bar{\Lambda} + \bar{\Sigma}^0)/N_{wound}$  (r.h.s.) as a function of the number of wounded nucleons  $N_{wound}$  for Pb+Pb collisions at 158 A·GeV at mid-rapidity from PHSD (blue solid lines) and HSD (red dashed-dotted lines) in comparison to the experimental data from the NA57 Collaboration [32] (open triangles) and the NA49 Collaboration [33] (solid dots). The HSD and PHSD calculations have an error of about 5–10% due to limited statistics.

(long dashed green line) and newly produced baryons + antibaryons (blue dashed line) as a function of time for the same reaction as before. We recall that the initial number of nucleons is 416 in this case. Slightly more than 1500 partons are produced during the passage time of the nuclei which disappear practically after 9 fm/c and essentially form mesons. The number of newly produced  $B + \bar{B}$  pairs is small at this energy but its flavor decomposition is quite interesting. An essential point here is that the number of final hadronic states is larger than the number of partons, i.e. there is a production of entropy in the hadronization process as pointed out before in Ref. [9]. This implies that in PHSD the second law of thermodynamics is not violated in the hadronization process!

### 3.2. Strangeness in PHSD

As found in Ref. [16] the impact of the partonic degrees of freedom in PHSD on the longitudinal rapidity distribution of protons, pions and kaons is only small in central Pb+Pb collisions at SPS energies from 40 to 158 A·GeV.

Additional experimental information is provided by the centrality dependence of the strange (and antistrange) baryon yield. In this respect we compare in Fig. 6 the multiplicities of  $(\Lambda + \Sigma^0)/N_{wound}$  (l.h.s.) and  $(\bar{\Lambda} + \bar{\Sigma}^0)/N_{wound}$  (r.h.s.) as a function of the number of wounded nucleons  $N_{wound}$  for Pb+Pb collisions at 158 A·GeV at mid-rapidity from PHSD (blue solid lines) and HSD (red dashed-dotted lines) to the experimental data from the NA57 Collaboration [32] (open triangles) and the NA49 Collaboration [33] (solid dots). The (green) full squares correspond to the 10% central data points at midrapidity from Ref. [34]. We mention that we employ the same definition of wounded nucleons  $N_{wound}$  as the NA49 Collaboration. Whereas the HSD and PHSD calculations both give a reasonable description of the  $\Lambda + \Sigma^0$  yield of the NA49 Collaboration, both models underestimate the NA57 data (open triangles) by about 30%. An even larger discrepancy in the data from the NA49 and NA57 Collaborations is seen for  $(\bar{\Lambda} + \bar{\Sigma}^0)/N_{wound}$  (r.h.s.); here the PHSD calculations give results which are in between the NA49 data (solid dots) and the NA57 data (open triangles). We also see that HSD underestimates the  $(\bar{\Lambda} + \bar{\Sigma}^0)$  midrapidity yield at all centralities.

The latter results suggest that the partonic phase does not show up explicitly in an enhanced production of strangeness (or in particular strange mesons and baryons) but leads to a different redistribution of antistrange quarks between mesons and antibaryons in the hadronization process.

#### 4. Summary

In this contribution we have presented a brief overview of the DQPM model and its results in comparison to lattice QCD. Furthermore, we have addressed relativistic collisions of Pb+Pb at SPS energies in the PHSD approach which includes explicit partonic degrees of freedom as well as dynamical local transition rates from partons to hadrons (20). The hadronization process conserves four-momentum and all flavor currents and slightly increases the total entropy since the 'fusion' of rather massive partons dominantly leads to the formation of color neutral strings or resonances that decay microcanonically to lower mass hadrons. Since this dynamical hadronization process increases the total entropy the second law of thermodynamics is not violated (as is the case for simple coalescence models incorporating massless partons).

The PHSD approach has been also applied to nucleus-nucleus collisions from 40 to 160 A·GeV in order to explore the space-time regions of 'partonic matter' [16]. We have found that even central collisions at the top SPS energy of  $\sim 158$  A·GeV show a large fraction of non-partonic, i.e. hadronic or string-like matter, which can be viewed as a 'hadronic corona'. This finding implies that neither purely hadronic nor purely partonic 'models' can be employed to extract physical conclusions in comparing model results with data.

On the other hand - studying in detail Pb+Pb reactions at 40, 80 and 158 GeV·GeV in comparison to the data from the NA49 Collaboration [16]- it is found that the partonic phase has only a very low impact on rapidity distributions of hadrons but a sizeable influence on the transverse-mass distribution of final kaons due to the parton interactions. The most pronounced effect is seen on the production of multi-strange antibaryons due to a slightly enhanced  $s\bar{s}$  pair production in the partonic phase from massive time-like gluon decay and a more abundant formation of strange antibaryons in the hadronization process. This enhanced formation of strange antibaryons in central Pb+Pb collisions at SPS energies by hadronization supports the early suggestion by Braun-Munzinger and Stachel [35, 36] in the statistical hadronization model - which describes well particle ratios from AGS to RHIC energies.

Some note of caution has to be stated here with respect to applications of PHSD at FAIR energies (5-40 A·GeV) since the partonic equation-of-state employed so far - as fixed to the lQCD results from Ref. [17] - describes a crossover transition between the hadronic and partonic phase while at lower SPS and FAIR energies a first-order phase transition and the appearance of a critical point in the QCD phase diagram are expected [37]. Such phenomena may not be described by the present realization of PHSD but need subtle extensions. Additionally, we have to mention that the high transition temperature from Ref. [17] might be questioned since related lattice calculations of the Wuppertal group in 2009 lead to lower critical temperatures [38]. Once the question of the 'proper  $T_c$  or critical energy density  $\epsilon_c$  is settled by the lattice community we might have to readjust the partonic equation-of-state in PHSD accordingly. On the other hand an application to RHIC energies is rather straight forward - except for a possible color-glass initial state - and detailed results from PHSD will be presented in a forthcoming study.

#### Acknowledgement

The authors are grateful to C. Blume, C. Höhne, O. Linnyk and S. Mattiello for valuable discussions.

## References

- [1] Shuryak E 2004 *Prog. Part. Nucl. Phys.* **53** 273
- [2] Thoma M H 2005 *J. Phys. G* **31** L7
- [3] Peshier A and Cassing W 2005 *Phys. Rev. Lett.* **94** 172301
- [4] Arsene I *et al.* 2005 *Nucl. Phys. A* **757** 1;  
Back B B *et al.* 2005 *Nucl. Phys. A* **757** 28;  
Adams J *et al.* 2005 *Nucl. Phys. A* **757** 102;  
Adcox K *et al.* 2005 *Nucl. Phys. A* **757** 184
- [5] Hirano T and Gyulassy M 2006 *Nucl. Phys. A* **769** 71
- [6] Hwa R C and Yang C B 2003 *Phys. Rev. C* **67** 034902;  
Greco V, Ko C M and Levai P 2003 *Phys. Rev. Lett.* **90** 202302
- [7] Fries R J, Müller B, Nonaka C and Bass S A 2003 *Phys. Rev. Lett.* **90** 202303
- [8] Lin Z-W *et al.* 2005 *Phys. Rev. C* **72** 064901
- [9] Cassing W and Bratkovskaya E L 2008 *Phys. Rev. C* **78** 034919
- [10] Juchem S, Cassing W and Greiner C 2004 *Nucl. Phys. A* **743** 92
- [11] Cassing W and Juchem S 2000 *Nucl. Phys. A* **665** 377
- [12] Ivanov Y B, Knoll J and Voskresensky D N 2000 *Nucl. Phys. A* **672** 313
- [13] Cassing W 2009 *E. Phys. J. ST* **168** 3
- [14] Cassing W 2007 *Nucl. Phys. A* **791** 365
- [15] Cassing W 2007 *Nucl. Phys. A* **795** 70
- [16] Cassing W and Bratkovskaya E L 2009 *Nucl. Phys. A* **831** 215
- [17] Cheng M *et al.* 2008 *Phys. Rev. D* **77** 014511
- [18] Cassing W and Bratkovskaya E L 1999 *Phys. Rep.* **308** 65
- [19] Peshier A 2004 *Phys. Rev. D* **70** 034016
- [20] Pisarski R D 1989 *Phys. Rev. Lett.* **63** 1129
- [21] Peshier A, Kämpfer B, Pavlenko O P and Soff G 1996 *Phys. Rev. D* **54** 2399
- [22] Bluhm M, Kämpfer B, Schulze R, Seipt D and Heinz U 2007 *Phys. Rev. C* **76** 034901
- [23] Aarts G and Martinez Resco J M 2002 *J. High Energy Phys.* **04** 054
- [24] Serot B D and Walecka J D 1988 *Adv. Nucl. Phys.* **16** 1
- [25] Maruyama T, Cassing W, Mosel U, Teis S and Weber K 1994 *Nucl. Phys. A* **573** 653
- [26] Larionov A B, Cassing W, Greiner C and Mosel U 2000 *Phys. Rev. C* **62** 064611
- [27] Bratkovskaya E L, Cassing W, Rapp R and Wambach J 1998 *Nucl. Phys. A* **634** 168
- [28] Dover C B, Heinz U, Schnedermann E and Zimanyi J 1991 *Phys. Rev. C* **44** 1636
- [29] Bengtsson H U and Sjöstrand T 1987 *Comp. Phys. Commun.* **46** 43
- [30] Falter T, Cassing W, Gallmeister K and Mosel U 2004 *Phys. Rev. C* **70** 054609
- [31] McLerran L 2007 *Nucl. Phys. A* **787** 1
- [32] Antinori F *et al.* 2004 *Phys. Lett. B* **595** 68
- [33] Anticic T *et al.* NA49 Collaboration 2009 *Phys. Rev. C* **80** 034906
- [34] Alt C *et al.* NA49 Collaboration 2008 *Phys. Rev. C* **78** 034918
- [35] Braun-Munzinger P *et al.* 2001 *Phys. Lett. B* **365** 1
- [36] Andronic A, Braun-Munzinger P and Stachel J 2006 *Nucl. Phys. A* **772** 167
- [37] Senger P *et al.* 2010 CBM Physics Book, *Springer*, in press.
- [38] Fodor Z and Katz S D 2009 *arXiv: 0908.334 [hep-ph]*